Mode conversion and period doubling in a liquid rubidium Alfvén-wave experiment with coinciding sound and Alfvén speeds

Stefani, F.; Forbriger, J.; Gundrum, T.; Herrmannsdörfer, T.; Wosnitza, J.;

Originally published:

December 2021

Physical Review Letters 127(2021), 275001

DOI: https://doi.org/10.1103/PhysRevLett.127.275001

Mode Conversion and Period Doubling in a Liquid Rubidium Alfvén-Wave Experiment with Coinciding Sound and Alfvén Speeds

F. Stefani,[1,*] J. Forbriger,[1] Th. Gundrum,[1] T. Herrmannsdörfer,[1] and J. Wosnitza[1,2]

[1] *Helmholtz-Zentrum Dresden-Rossendorf, Bautzner Landstr. 400, 01328 Dresden, Germany*
[2] *Institut für Festkörper- und Materialphysik und Würzburg-Dresden Cluster of Excellence ct.qmat, TU Dresden, 01062 Dresden, Germany*

(Dated: November 25, 2021)

We report Alfvén-wave experiments with liquid rubidium at the Dresden High Magnetic Field Laboratory (HLD). Reaching up to 63 T, the pulsed magnetic field exceeds the critical value of 54 T at which the Alfvén speed coincides with the sound speed. At this threshold we observe a period doubling of an applied 8 kHz CW excitation, which is consistent with the theoretical expectation of a parametric resonance between magnetosonic waves and Alfvén waves. Similar mode conversions are discussed as a possible mechanism for heating the solar corona.

Since their discovery by Hannes Alfvén in 1942 [1], Alfvén waves have played an ever increasing role in understanding astrophysical and fusion-related plasmas. They are, in particular, one of the main ingredients to explain the dramatic heating of the solar corona [2] and to accelerate the solar wind [3], they are found in the Earth's ionosphere [4], and they are being employed for the heating of fusion plasmas [5, 6]. More generally, Alfvén waves serve as a reference paradigm for a variety of waves and instabilities in rotating magnetized plasmas or liquid metals, in particular the magnetorotational instability [7, 8] and torsional oscillations in the Earth's outer core [9].

Laboratory experiments on Alfvén waves in liquid mercury [10] and sodium [11] had started soon after Alfvén's theoretical prediction. Since those early times, many Alfvén wave experiments have been carried out, both with liquid metals [13, 14, 32] and, more extensively, with plasmas [15, 16]. Recently, liquid-metal experiments were resumed in order to study Alfvén waves with pulsed excitations [31], as well as torsional Alfvén waves in spherical geometry [18].

The recent progress in generating pulsed magnetic fields beyond $B = 90\,\mathrm{T}$ [19, 20] opens up a completely new prospect for Alfvén-wave experiments with liquid metals. It is at those fields (51 T for caesium and 54 T for rubidium) that the Alfvén speed $v_\mathrm{a} = B/(\mu_0\rho)^{0.5}$ in higher alkali metals crosses the sound speed c_s. This threshold (which in plasma physics is also related to plasma-β unity, β being the ratio of thermal to magnetic pressure), is of key importance for the mutual transformability of Alfvén waves and (slow and fast) magnetosonic waves [21, 22] (see [23], Sec. I for more details on the relation of these three types of waves). Such transformations at the so-called "magnetic canopy" are one possible candidate to explain the heating of the solar corona [24, 25]. One particular effect predicted to occur at this threshold is the transfer of the energy of magnetosonic waves of a given frequency into Alfvén waves of half that frequency (period doubling). Thereby, the Alfvén wave drives the sound wave through the ponderomotive force, while the sound wave returns energy back to the Alfvén wave through the parametric (swing) influence. As a result, the two waves alternately exchange their energy during propagation [26].

In this Letter, we report experimental evidence for the occurrence of this period-doubling effect in an Alfvén-wave experiment with liquid rubidium. Using one of the pulsed-field coils at the Dresden High Magnetic Field Laboratory (HLD), the achieved maximum field value of 63 T exceeds the threshold $v_\mathrm{a} = c_\mathrm{s}$, reached at 54 T, by 17 %. Yet, the pulsed character of the field entails various technical challenges, among them a huge contribution of the magnetic-flux derivative to the voltage induced in the pick-up coils (an effect that is, by and large, overcome by using compensation coils), and a significant pressure buildup in the liquid metal leading to an uncontrolled background flow field. A further challenge is the limited size of the available experimental volume: the cold-bore diameter in the 70 T long pulse coil of the HLD [19] is 24 mm. Since the copper-alloy coil of the large magnet is immersed into liquid nitrogen, the (warm) rubidium experiment has to be shielded thermally from this cold surrounding by a double-wall Dewar lance which reduces the available diameter further. A holder for the pick-up coils is also necessary, so that the outer diameter of the stainless steel container for the Rubidium is 12 mm. As the pressure in the liquid, arising from the steep increase of the pulsed magnetic field, reaches values in the order of 50 bar, a container wall thickness of 1 mm is necessary, which reduces the ultimately available diameter d of the rubidium column to 10 mm. The height of this column, limited by the homogeneity region of the magnetic field, has been chosen as 60 mm. The central part of the setup, with the container, the coil holder, the pick-up coils and the electric-potential probes is visualized in Fig 1.

Figure 2 shows some chief results of one experimental run, carried out at a temperature of 50°C at which rubidium is liquid. After releasing, at $t = 20\,\mathrm{ms}$, the energy from the capacitor bank (charged with 22 kV) the

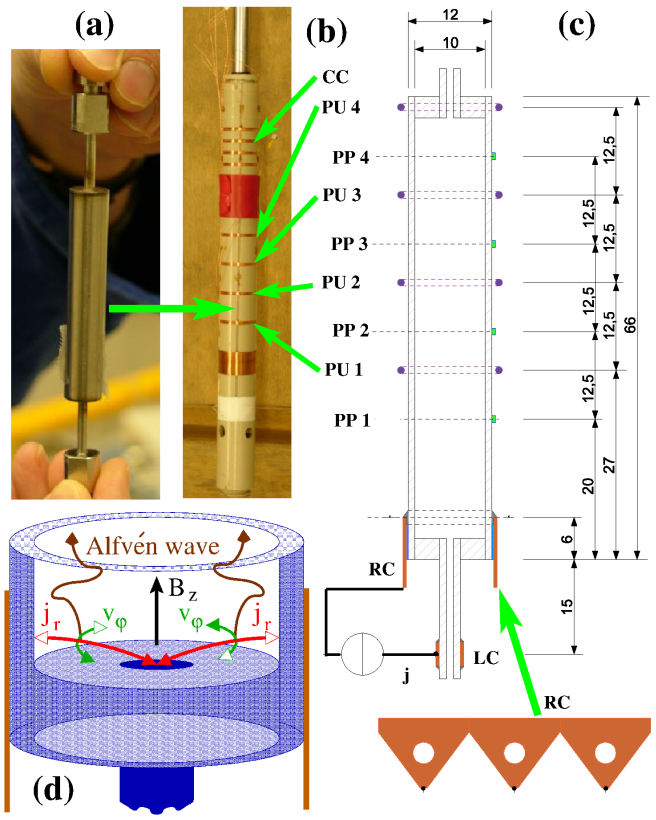

FIG. 1. Experimental setting: (a) Stainless-steel container filled with rubidium. (b) Holder with four pick-up coils (PU 1 - PU 4), and four compensation coils (CC). (c) Geometrical details of the construction. PP 1 - PP 4 denote four electric-potential probes soldered on the container. The three orange triangles indicate the rim contacts (RC) encircling the bottom part of the container. LC is the lower contact. All sizes are in mm. (d) Schematic for the driving of the torsional Alfvén wave in the lower part of the container.

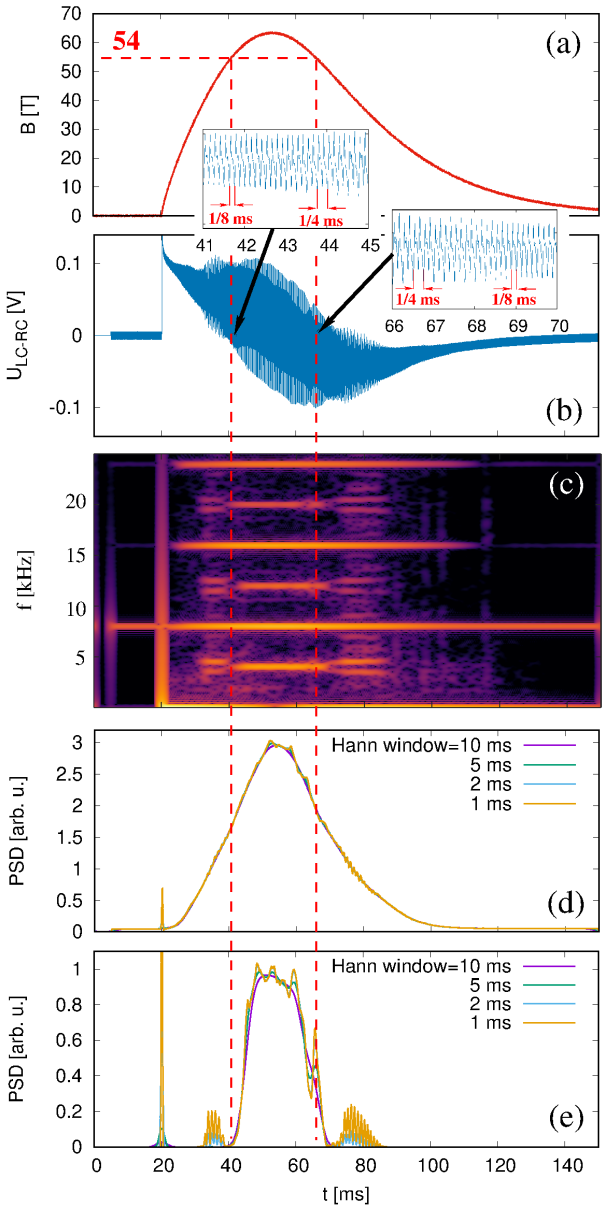

FIG. 2. Time dependence of the pulsed magnetic field (a), and of the voltage measurements at the lower contact (b). The red dashed lines indicate the instants where the critical field strength of 54 T is crossed. The insets of (b) detail the two transition regions, where the double-period signal starts and ceases to exist. Gabor transform (c) of the signal from (b), with a von Hann window width of 5 ms. Amplitude of the 8 kHz (d) and the 4 kHz (e) stripe from (c), for different choices of the von Hann window width. The PSD units of (d) and (e) are arbitrary, but consistent among each other.

axial magnetic field [Fig. 2(a)] increases swiftly to attain its maximum value of 63.3 T at $t = 53$ ms. From there on, the field declines slowly, reaching a value of 2.1 T at the end of the interval considered here ($t = 150$ ms). The period during which the critical value of 54 T is exceeded ranges from 40.5 ms until 66 ms, as indicated by the dashed red lines. During the entire experiment, a controlled current source (Agilent 33220A and Rohrer PFL-2250-28-UDC415-DC375) provided a very stable sinusoidal CW current (not shown) with constant amplitude of 5 A and frequency 8 kHz, which was applied between the lower contact (LC) and the three contacts (RC) encircling the lower rim of the container [illustrated at the lower part of Fig. 1(c)]. The corresponding current density $\mathbf{j}_r$, which is concentrated in the bottom layer of the rubidium where it is basically directed in radial direction, generates together with the strong vertical field $\mathbf{B}_z$ an azimuthal Lorentz force density $\mathbf{f}_\varphi = \mathbf{j}_r \times \mathbf{B}_z$ that is supposed to drive a torsional Alfvén wave in the fluid [see Fig. 1(d)].

The voltage $U_{\mathrm{LC-RC}}$ measured between the contacts LC and RC comprises three contributions: First, a significant electro-motive force (emf) $\mathbf{v}_\varphi \times \mathbf{B}_z$ arising from the interaction of the toroidal velocity $\mathbf{v}_\varphi$ of the generated torsional (Alfvén) wave with the axial magnetic

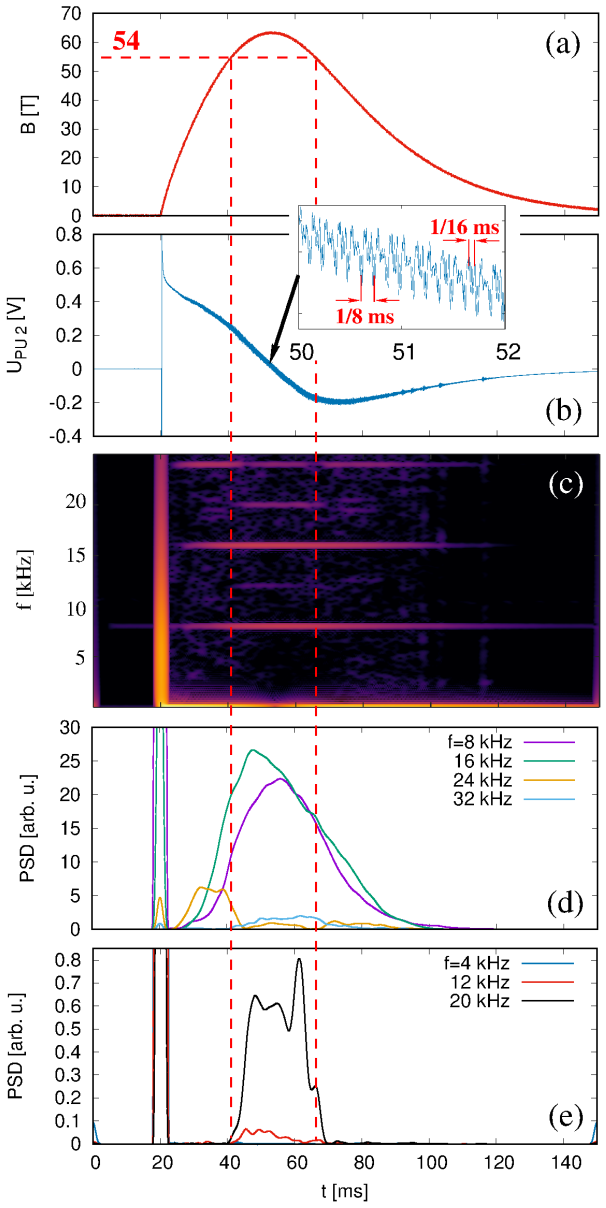

FIG. 3. Time dependence of the applied magnetic field (a), and of the (compensated) voltage measurement at the pick-up coil PU 2 (b). The red dashed lines indicate the instants where the critical field strength of 54 T is crossed. The inset of (b) shows the region of highest field, where a significant contribution of a 16 kHz signal is visible. Gabor transform (c) of the signal from (b), with a von Hann window width of 5 ms. Amplitudes of the 8 kHz, 16 kHz, 24 kHz, and 32 kHz stripes (d) and of the 4 kHz, 12 kHz, and 20 kHz stripes (e) from (c). The PSD units of (d) and (e) are arbitrary, but consistent among each other.

field $\mathbf{B}_z$. Second, the usual Ohmic voltage drop [giving an amplitude of approximately 5 mV, as seen at at the start and end of the magnetic-field pulse when the magnetic field is close to zero, Fig. 2(b)]. Third, a certain long-term trend resulting from the time derivative of the pulsed field (which is still induced in the wire system used for the electric contacts that is oriented not perfectly radially).

Already without having performed detailed numerical analyses, we can at least plausibilize the measured oscillation amplitude of this emf: with an applied current amplitude of 5 A, we obtain (for the given contact geometry) a current density of $j_r \approx 100\,\mathrm{kA/m^2}$, leading (with $B_z = 50\,\mathrm{T}$ and a density of $\rho = 1490\,\mathrm{kg/m^3}$) to an azimuthal acceleration of $a_\varphi \approx 3000\,\mathrm{m/s^2}$. Acting over half an excitation period (1/16 ms), this acceleration can generate flow velocities of $v_\varphi \approx 20\,\mathrm{cm/s}$, which in turn induce (integrated over the container's radius of $r = 5\,\mathrm{mm}$) an emf of $v_\varphi B_z r \approx 50\,\mathrm{mV}$. This estimation is well compatible with the amplitude of the voltage oscillation as seen in the high-field segment of Fig. 2(b). Given the high quality of the Alfvén wave resonator, as indicated by the Lundquist number $S = \sigma\sqrt{\mu_0/\rho}B_z d = 67.7$ (taken at 54 T, with the electrical conductivity $\sigma = 4.32\,\mathrm{MS/m}$), this good correspondence with our simple estimate is not that surprising. Accordingly, in [23] (which includes Refs. [28–30]), Sec. II, we show how Alfvén waves move in axial direction, and derive their speed by correlating signals from neighboring potential probes. While for low magnetic fields the Alfvén speeds derived for the 8 kHz mode agree very well with the theoretical ones, for increasing magnetic field (leading to wavelengths which do not fit anymore into the device), this time-of-flight measurement delivers progressively reduced values (Fig. S8).

The measured voltage $U_{\mathrm{LC-RC}}$ is now analyzed in detail by means of a windowed Fourier transform (or Gabor transform, using the "ltfat" toolbox in Octave [27]). For a von Hann window width of 5 ms, Fig. 2(c) shows the arising spectrogram (i.e., the Power Spectral Density (PSD) over time), restricted here to the frequency range $0 - 25\,\mathrm{kHz}$, with a resolution of 100 Hz. The dominant feature of this spectrogram is, not surprisingly, the 8 kHz signal, whose time dependence is separately plotted in Fig. 2(d) for four different widths of the von Hann window. Since the amplitude of the velocity induced emf increases smoothly with B_z, there is a negligible dependence on the window width. Another unsurprising feature seen in Fig. 2(c) is the appearance of various overtones of 8 kHz.

What is surprising, however, is the appearance of a strong *period-doubling* 4 kHz line (and its overtones) which shows up nearly exclusively in the time interval when the field is equal to, or larger than, the critical value of 54 T. Figure 2(e) illustrates this restriction quite clearly. Notable is a certain asymmetry in time: after crossing the threshold, the 4 kHz mode seems to require some time to fully develop, while it extends slightly beyond the end of the interval. Note also, exclusively at the (slowly) decreasing branch, the special peak appearing very close to $B = 54\,\mathrm{T}$, which is not visible on the (steeply) increasing branch. The remarkable cleanliness

and the significant PSD amplitude of this 4 kHz mode (reaching one third of the PSD of the 8 kHz mode), is also highlighted in the two insets of Fig. 2(b) where the initial onset and the later decay of that mode are shown. More details are shown in [23], Sec. III, where we discuss in particular the very stable phase relation between the 4 kHz and the 8 kHz mode. We also hint to the obvious splitting of the 4 kHz mode which occurs shortly before and after the critical thresholds [Fig. 2(c)] (see [23], Sec. III for more details and a preliminary explanation of this effect.)

With Fig. 3, we turn now to the voltage measurements from the pick-up coil PU 2 that is located slightly above mid-height of the container (the signals of the other PU's are similar). Despite a significant reduction due to the use of a compensation coil, the dominant part of this signal [Fig. 3(b)] is still coming from the time derivative of the pulsed magnetic field [note the similarity of this shape with the shape of the low-frequency part in Fig. 2(b)]. Superposed on that, we observe a high-frequency part comprising the usual 8 kHz, and a second-harmonic 16 kHz signal of approximately the same amplitude. How to explain that mixture? To start with, the voltage in the pick-up coils results from time derivatives of azimuthal currents $\mathbf{j}_\varphi$ which are typically produced by the induction effect $\mathbf{v}_\mathrm{r} \times \mathbf{B}_\mathrm{z}$ of radial flow components $\mathbf{v}_\mathrm{r}$ with the axial field $\mathbf{B}_\mathrm{z}$. That flow component, in turn, is intimately connected with radial and axial gradients of the pressure p, and is, therefore, indicative of the presence of magnetosonic waves. Hence, the appearance of the 16 kHz signal is a well-known consequence of the quadratic dependence of the pressure on the magnetic-field perturbation of the Alfvén wave, as already discussed for the gallium experiment of Iwai et al. [14]. The amplitude of the original driving frequency (8 kHz) is comparable to that of the second harmonic [see Fig. 3(d)], quite in contrast to [14], where it was significantly larger (as a consequence of the different directions of the driving force, which pointed in y direction in [14], but is torsional in our case). At any rate, the third and fourth harmonics are already much smaller.

Remarkable here is the nearly complete absence of any 4 kHz signal, and only very minor contributions from the higher $(2n+1)\times 4$ kHz harmonics [note the significant differences of the PSD units between Figs. 3(d) and 3(e)]. This absence of any *pressure related* 4 kHz signal is in stark contrast to the quite significant share of this frequency band in the voltage measurements at $B_\mathrm{z} \geq 54$ T [Fig. 2(e)], which we attribute to the emergence of a new torsional Alfvén wave at the 54 T threshold related to $v_\mathrm{a} = c_\mathrm{s}$.

In Fig. 4, we translate those time series into corresponding magnetic-field dependencies, including both the increasing and decreasing branches. Based on the data from Fig. 2, Fig. 4(a) confirms, first, the quadratic dependence of the PSD of the driven 8 kHz mode (with

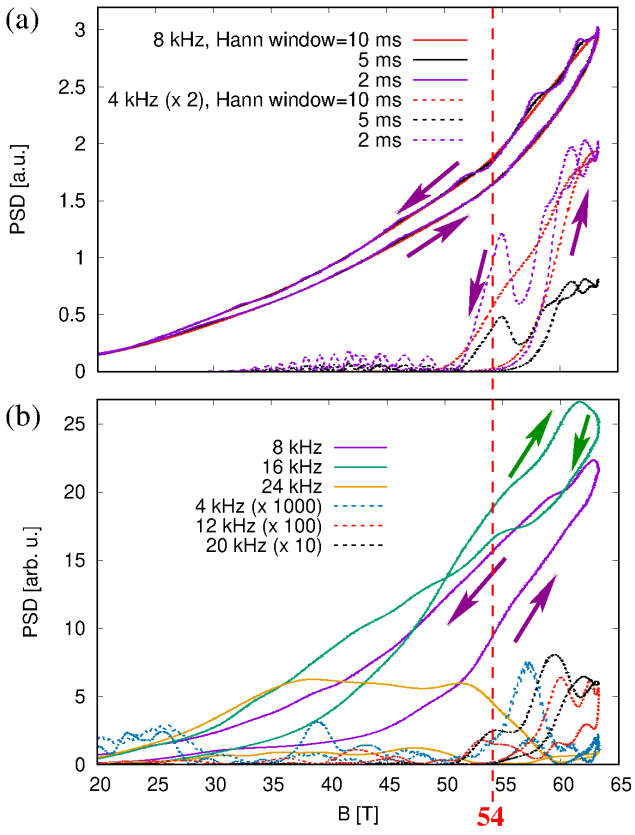

FIG. 4. Dependence of various measured signals on the magnetic field. (a) PSD of the 8 kHz and the 4 kHz coefficients of the voltage $U_{\mathrm{LC-RC}}$ from Figs. 2(d) and 2(e) for three different von Hann windows. (b) PSD of the 8, 16, and 24 kHz signals from Fig. 3(d), and of the 4, 12, and 20 kHz signals from Fig. 3(e). The arrows indicate rising and falling branches of the pulsed magnetic field.

only a slight difference between the increasing and the decreasing branch), which one expects from the linear dependence of the torsional velocity on B_b as plausibilized above. Second, we observe a clear peak of the 4 kHz signal close to 54 T coming from the decreasing branch, and another peak behind, coming from the increasing branch. Note that this persistence of the 4 kHz signal for $v_\mathrm{a} > c_\mathrm{s}$ is not readily explainable by the parametric resonance model of [26]. In view of the weakness of the magnetic-field perturbations (the estimated velocity scale of the Alfvén wave implies a corresponding magnetic-field perturbation of $b = v_\varphi(\mu_0\rho)^{0.5} \approx 9$ mT, which is only 0.02 per cent of the applied field), it cannot be related to a simple broadening of the resonance peak due to nonlinear effects. For the moment, we tend to attribute this second peak either to the transient behavior during the fast increasing branch or to problems in connection with the rather long wavelengths of the 8 and 4 kHz modes, for which the assumption of freely travelling waves [26] has to be modified.

Figure 4(b) shows the PSD dependence on the magnetic field for the signal of the pick-up coil PU 2 from Fig. 3. Evidently the 8 and 16 kHz signals look quite similar, with some differences in the up-down relation which still remain to be understood. At any rate, the 4, 12, and 20 kHz curves are extremely small (note, in particular, the factor 1000 by which which the 4 kHz signal must be multiplied to become visible).

To the best of our knowledge, we have carried out the first systematic Alfvén wave experiment where the "magical" threshold $v_a = c_s$ has been crossed. In contrast to many plasma experiments, which are usually carried out at $v_a > c_s$, i.e., plasma $\beta < 1$ (but see [33–35] for interesting exceptions, with some evidence for a shear wave being converted from a compressional wave [34]), liquid metal experiments were up to present limited to the region with $v_a \ll c_s$. Using liquid rubidium in the high pulsed fields available at the HLD, we were able to exceed this threshold by some 17 percent. Our main observation was the sudden appearance (at $v_a = c_s$) of a period-doubled 4 kHz mode, which we interpret as a new torsional Alfvén wave arising by parametric resonance, or swing excitation [26], from the usual 8 kHz magnetosonic wave. Admittedly, the first realization of this phenomenon under strongly transient experimental conditions demands for substantial numerical support. Complementary experiments with longer pulses, and higher frequencies connected with shorter wavelengths, would also be desirable for a better understanding of the unanticipated wave behavior in the $v_a > c_s$ regime.

We acknowledge support of the HLD at HZDR, a member of EMFL, and the DFG through the Würzburg-Dresden Cluster of Excellence on Complexity and Topology in Quantum Matter - *ct.qmat* (EXC 2147, Project No. 390858490). F.S. acknowledges further support by the European Research Council (ERC) under the European Union's Horizon 2020 Research and Innovation Programme (Grant No. 787544). We thank Jürgen Hüller for his assistance in the adventurous filling procedure of the rubidium container, and Frank Arnold, Carsten Putzke, Karsten Schulz, and Marc Uhlarz for their help in preparing and carrying out the experiment.

* F.Stefani@hzdr.de

[1] H. Alfvén, Nature **150**, 405 (1942).
[2] S. Tomczyk, S. W. McIntosh, S. L. Keil, P. G. Judge, T. Schad, T. H. Seeley, and J. Edmondson, Science **317**, 1192 (2007).
[3] J. C. Kasper et al., Nature **576**, 228 (2019).
[4] R. L. Lysak, C. L. Waters, and M. D. Sciffer, J. Geophys. Res.: Space Phys. **118**, 1514 (2013).
[5] A. Fasoli et al., Nucl. Fusion **35**, 1485 (1995).
[6] T. Intrator et al., Phys. Plasmas **2**, 2263 (1995).
[7] S. A. Balbus and J. F. Hawley, Astrophys. J. **376**, 214 (1991).
[8] F. Stefani, T. Gundrum, G. Gerbeth, G. Rüdiger, M. Schultz, J. Szklarski, and R. Hollerbach, Phys. Rev. Lett. **97**, 184502 (2006).
[9] N. Gillet, D. Jault, E. Canet, and A. Fournier, Nature **465**, 74 (2010).
[10] S. Lundquist, Nature **164**, 146 (1949).
[11] B. Lehnert, Phys. Rev. **94**, 815 (1954).
[12] A. Jameson, J. Fluid Mech. **19**, 513 (1964).
[13] W. F. Druyvesteyn, C. A. A. J. Greebe, A. J. Smets, and R. Ruyg, Phys. Lett. **27A**, 301 (1968).
[14] K. Iwai, K, Shinya, K. Takashi, and R. Moreau, Magnetohydrodynamics **39**, 245 (2003).
[15] W. Gekelman, J. Geophys. Res., **104**, 14417 (1999).
[16] W. E. Amatucci, Radio Sci. Bull. **319**, 32 (2006).
[17] T. Alboussiere, P. Cardin, F. Debray, P. La Rizza, J.-P. Masson, F. Plunian, A. Ribeiro, and D. Schmitt, Phys. Fluids **23**, 096601 (2011).
[18] Z. Tigrine, H.-C. Nataf, N. Schaeffer, Ph. Cardin, and F. Plunian, Geophys. J. Int. **219**, S83 (2019).
[19] J. Wosnitza et al., J. Magn. Magn. Mat. **310** 2728 (2007).
[20] S. Zherlitsyn, B. Wustmann, T. Herrmannsdörfer, and J. Wosnitza, IEEE Trans. Appl. Supercond. **22**, 4300603 (2012).
[21] T. V. Zaqarashvili, R. Oliver, and J. L. Ballester, Astron. Astrophys **456**, L13 (2006).
[22] A. Warmuth, G. Mann, Astron. Astrophys. **435** 1123 (2005).
[23] See Supplemental Material at http://link.aps.org/supplemental/...
[24] J. V. Hollweg, S. Jackson, and D. Galloway, Solar Phys. **75**, 35 (1980).
[25] T. J. Bogdan et al., Astrophys. J. **599**, 626 (2003).
[26] T. V. Zaqarashvili and B. Roberts, Astron. Astrophys. **452**, 1053 (2006).
[27] https://octave.sourceforge.io/ltfat/index.html
[28] R. M. Kulsrud, *Plasma Physics for Astrophysics*, (Princeton University Press, Princeton and Oxford, 2005).
[29] F. Stefani and G. Gerbeth, Inverse Probl. **15**, 771 (1999).
[30] R. T. Jacobs, T. Wondrak, and F. Stefani, COMPEL **37**, 1366 (2018).
[31] T. Alboussiere, P. Cardin, F. Debray, P. La Rizza, J.-P. Masson, F. Plunian, A. Ribeiro, and D. Schmitt, Phys. Fluids **23**, 096601 (2011).
[32] A. Jameson, J. Fluid Mech. **19**, 513 (1964).
[33] M. Cekic, B. A. Nelson, and F. L. Ribe, Phys. Plasmas **4**, 392 (1992).
[34] S. Okada et al., Nucl. Fusion **41**, 625 (2001).
[35] K. Flanagan, J. Milhone, J. Egedal, D. Endrizzi, J. Olson, E. E. Peterson, R. Sassella, and C. B. Forest, Phys. Rev. Lett. **125**, 135001 (2020).